Journal of Photochemistry and Photobiology A: Chemistry 221 (2011) 187–193

Contents lists available at ScienceDirect

Journal of Photochemistry and Photobiology A: Chemistry

journal homepage: www.elsevier.com/locate/jphotochem

Wide-field Rayleigh scattering imaging and spectroscopy of gold nanoparticles in heavy water under laser trapping

Takayuki Uwada[a,b,*], Teruki Sugiyama[b,c], Hiroshi Masuhara[a,b,*]

[a] Department of Applied Chemistry and Institute of Molecular Science, National Chiao Tung University, Hsinchu 30010, Taiwan
[b] Graduate School of Materials Science, Nara Institute of Science and Technology, Ikoma, Nara 630-0192, Japan
[c] Instrument Technology Research Center, National Applied Research Laboratories, Hsinchu 30076, Taiwan

ARTICLE INFO

Article history:
Available online 13 June 2011

Keywords:
Gold nanoparticle
Rayleigh scattering
Laser trapping
Nanomaterial assembling

ABSTRACT

We demonstrated wide-field Rayleigh scattering spectroscopy and imaging of gold nanoparticle trapping upon a focused near-infrared laser irradiation under dark-field illumination. The migration, trapping, and assembling behavior of gold nanoparticles were examined at single nanoparticle level at the focus spot and its surrounding area in heavy water. It is clarified that particle migration to the laser spot within the focal plane is not appreciable while scattering force drives the migration vertically along the direction of light propagation. The gradient force at the focus point and the scattering force are theoretically estimated to be 3.1 and 0.17 pN, which are consistent with the direct observation. Analysis of light scattering intensity fluctuation at the focus shows that three nanoparticles can be trapped at most, which is well supported by light scattering spectral measurement. The particle existence probability at the focus is estimated as a function of lateral distance from the focus, and is compared with numerically obtained photon pressure potential.

1. Introduction

Laser trapping based on the gradient and scattering forces of photon pressure was applied initially to micrometer-sized objects such as microspheres, microbeads, and biological cells at the laser focus spot since the first demonstration by Ashkin [1–4]. Currently, this technique has become indispensable for cell biology, single biomolecule study, micromachine operation, and so on. In the past two decades, the target of the laser trapping has been expanded from micrometer-sized objects to nanomaterials [5,6], and a variety of the applications in physics, chemistry, and biology have been explored [7]. One of the most conventional applications of the photon pressure to nanomaterials is their assembling at the laser focus. Since the size of laser focus spot (~1 μm) is much larger than that of nanomaterials, a number of nanomaterials can be trapped simultaneously, accumulated, and assembled in the single spot. Indeed, the photon pressure was successfully realized assembling of metallic nanoparticles [8–10], latex nanoparticles [11], semiconductor nanowires [12], polymers [13–17], proteins [18], and molecular aggregates [19,20] in solution. In particular, the present authors (T.S. and H.M.) demonstrated for the first time photon pressure-induced spatiotemporal crystallization [21,22] of amino acids at air/solution interface, implying further potential application of photon pressure from nanomaterial to molecular assembling.

In most of the reported studies, much attention is paid to dynamic processes of nanomaterial aggregation just at the focus spot, and the migration process is rarely considered, as the studies were usually performed on confocal microscopic measurement at the trapping laser focus. In situ observation of the whole assembling sequence, not only at the focus spot but also in the surrounding area, is considered to be important and indispensable to clarify the laser trapping and assembling dynamics. From this viewpoint, we have started our study to dynamically visualize what happen outside the focus point at single nanoparticle/molecule level by utilizing wide-field microscopic imaging technique.

In this work, we report on laser trapping properties of gold nanoparticles dispersed in heavy water (D_2O). The solvent was chosen to suppress temperature elevation as compared to light water (H_2O), where the overtone band of OH bond absorbs 1064 nm photon leading to local heating and modifications of the solubility, viscosity, and density and so on. Thus, the study on D_2O solution can elicit the role of photon pressure with less temperature effect. Because of the large light scattering cross section, gold nanoparticles can be proper optical probes to study particle transportation, trapping, and assembling sequence at single particle level. Additionally, laser trapping of gold nanoparticles is of great interest for the fundamental and application aspects in plasmonics and in surface enhanced spectroscopy [23–25]. The

* Corresponding authors at: Department of Applied Chemistry and Institute of Molecular Science, National Chiao Tung University, Hsinchu 30010, Taiwan.
Tel.: +886 3 5712121x56595.
E-mail addresses: uwada@mail.nctu.edu.tw (T. Uwada), sugiyama@itrc.narl.org.tw (T. Sugiyama), masuhara@masuhara.jp (H. Masuhara).

1010-6030/$ – see front matter © 2011 Elsevier B.V. All rights reserved.
doi:10.1016/j.jphotochem.2011.05.015

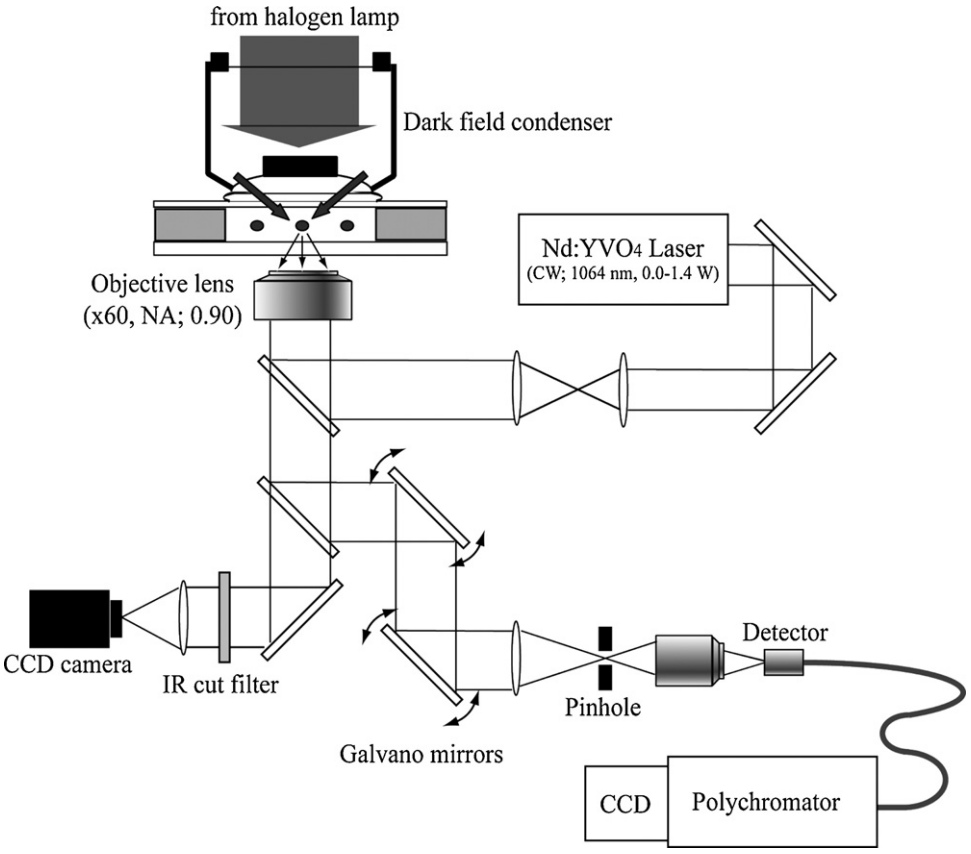

Fig. 1. A schematic illustration of wide-field light scattering microspectroscopic imaging system.

manipulation, rotation, and followed by assembling realized by laser trapping can control geometric structure of gold nanoparticles, leading to tuning of the optical property and creating a hot spot. Here, two-dimensional wide-field Rayleigh scattering imaging and spectroscopy of gold nanoparticles at specific positions including focus spot and the surroundings were carried out. A role of photon pressure to nanoparticle migration towards the focus of trapping laser followed by assembling was examined and considered, which will be helpful to understand molecule/particle migration dynamics in laser trapping induced assembling and crystallization.

2. Experimental setup

Gold colloidal solution (mean diameter 60 nm, EMGC60, British Biocells) was purchased and its solvent was replaced with heavy water (99.8%, Aldrich) by repeating centrifuge separation several times. Then it was diluted to the concentration roughly 5.0×10^9 particles/ml. It was confirmed by UV–vis absorption spectroscopy (V-670, JASCO) that no aggregation occurred during and after the centrifuging process. A glass substrate was sealed with a CoverWell perfusion chamber (depth, 1.0 mm; diameter, 20 mm; GraceBio-Labs) and its inside was filled with the colloidal solution, and was settled on a sample stage of an inverted optical microscope (IX71, Olympus).

A schematic experimental setup is depicted in Fig. 1. To create the trapping potential, a CW Nd:YVO_4 laser beam with a linear polarization (wavelength: 1064 nm, J20 I-BL-106C, Spectra Physics) was coupled into a high numerical objective lens (UPLSAPO 60×, NA 0.90, Olympus) and was focused into the sample solution [26]. The laser focus position was verified from the reflection spot on glass substrate using a Visible-NIR digital CCD camera (CV-A50IRC, JAI). The trapping laser power was measured after the objective by a power meter (842-PE, Spectra Physics). The focus height was adjusted mechanically by using a stepping motor-driven objective lens positioner. The sample on the microscope was illuminated with dark-field setup using white light from a 100-W halogen lamp via an oil-immersion dark-field condenser lens (U-DCW, NA 1.35-1.20, Olympus).

In dark-field illumination, single gold nanoparticles are recognized as individual bright points in dark background [27]. Scattered light from gold nanoparticles was collected with the same objective lens for laser trapping and was sent to the digital CCD camera mentioned above through a NIR cut filter (FES-0900, Semrock) to avoid reflection of laser light. For spectroscopic measurement, the scattered light was spatially selected by using an imaging pinhole (300 μm radius) through a pair of scanning galvano mirrors built in the confocal unit (FV300, Olympus) and was sent to a polychromator (SpectraPro 2300i, Princeton) coupled with a CCD camera (PIXIS 400, Princeton). The spatial resolution of the spectroscopic measurement is determined as roughly 500 nm in lateral dimension based on a measurement of single gold nanoparticle fixed on a glass substrate. The galvano mirrors in the confocal unit realize position-selective measurement, so that spectroscopic investigation from the focus position to the outside by changing the distance is possible while the trapping laser spot is fixed.

3. Results and discussion

Firstly, we observe lateral-directional motion of gold nanoparticles under laser trapping condition. Fig. 2 represents wide-field Rayleigh scattering images of gold nanoparticles dispersed in D_2O after 10 s laser exposure at 700 mW and their line profiles. The laser focus height was fixed at 100 μm above the surface of the

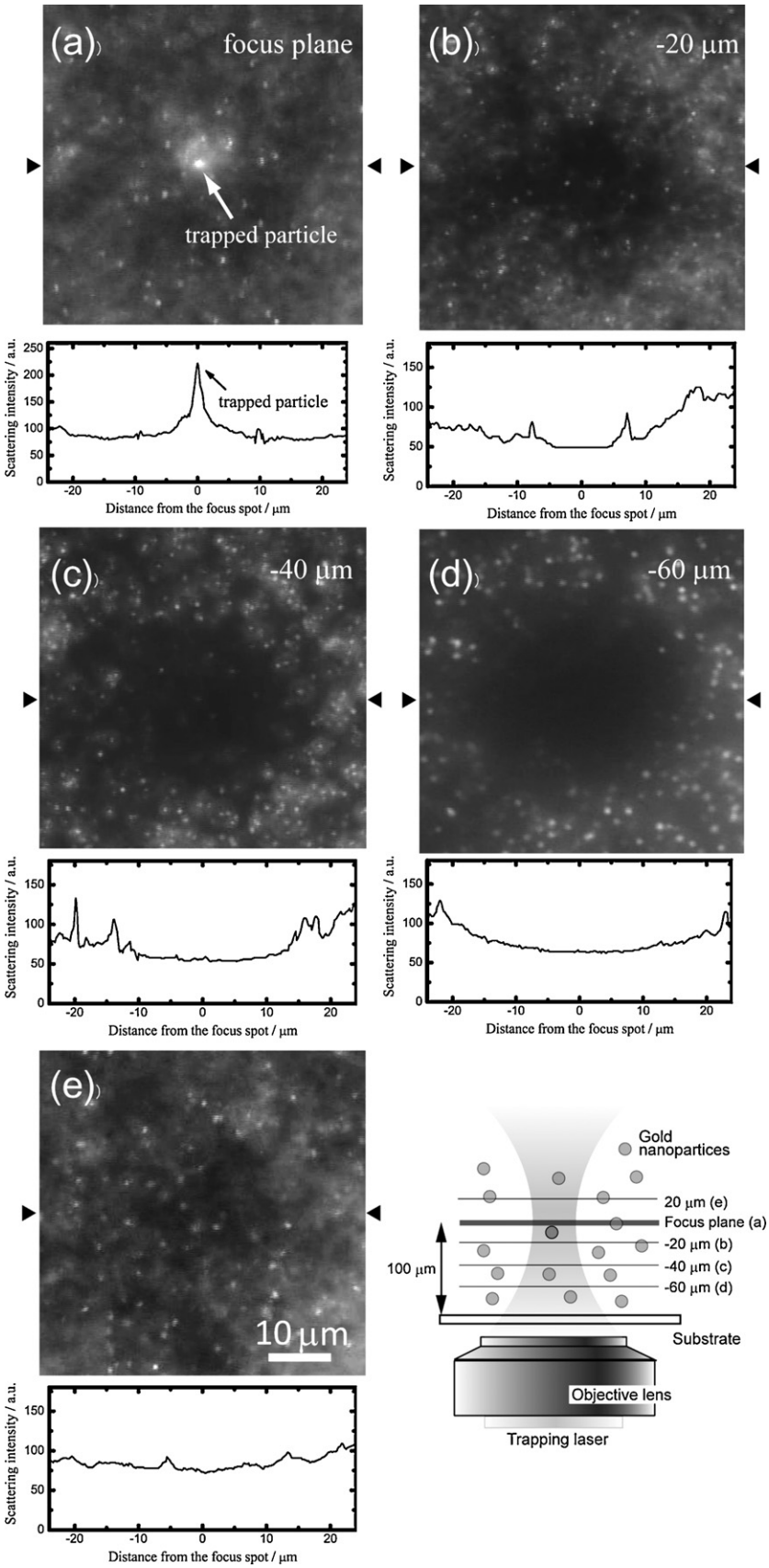

Fig. 2. Wide-field Rayleigh scattering images of gold nanoparticles dispersed in heavy water under laser trapping and line profiles of their intensity at (a) the focus plane, and (b) −20 μm, (c) −40 μm, (d) −60 μm below, and (e) +20 μm above the focus, respectively. The line profiles are taken between triangles indicated in the images across the focus spot. The focus height and the trapping laser power were set to 100 μm and 700 mW, respectively. A schematic illustration of the imaging plane is depicted at the lower right.

glass substrate. The dark-field illumination enables us to recognize nanoparticles as bright spots in dark background. At the focus plane (Fig. 2(a)), individual moving points were observed widely, indicating Brownian motion of gold nanoparticles. At the focus spot, a single bright point was clearly observed in the image and is shown in the corresponding line profile and its intensity decreased or increased over time, but its motion was suppressed compared to the surrounding particles. This means that the gold nanoparticles were optically trapped, that is, the particles were pulled into the center of beam spot and fixed there by strong electric field gradient of the tightly focused laser beam, i.e., gradient force [3]. During the laser trapping, gold nanoparticles in the surrounding of the focus spot showed Brownian motion but rarely moved to the focus, while trapped particles sometimes went away from the focus to the surrounding. We consider that lateral particle transfer to the focus spot is not dominant for laser trapping in D_2O.

Secondly, gold nanoparticles motion along the vertical direction was examined under laser trapping condition. As we employed an identical objective lens for both laser trapping and light scattering imaging, we cannot observe the vertical particle migration dynamically during laser trapping. Here we evaluated the vertical particle distribution as follows; the laser was irradiated until the steady state is attained, it was immediately turned off after observing the nanoparticle trapping, and the observation plane was shifted from 100 μm above the substrate surface to lower or higher position. The observed images are given in Fig. 2(b)–(d), where the observation plane was shifted to −20, −40, and −60 μm from the focus spot, respectively. Below the trapping laser focus, it was found that dark circular area around the laser axis existed at each plane. Before trapping laser was introduced, wide-field images gave a homogeneous distribution of shining and moving spots, so that this particle-deficient area was generated by laser irradiation. The area was observed for a few tens seconds until particles in the surroundings diffused into and filled up the area. It is also revealed that the area became larger with disengaging from the focus position. We consider that the scattering force can induce transfer of particles to far away, larger than several tens μm, and the diameters of the deficient area at each height were roughly estimated at 12, 24, and 35 μm, respectively. Thus, the deficient volume is considered to have a circular–cone shape, which may reflect propagating way of trapping laser beam.

The present results suggests that scattering force of the trapping laser beam pushes the particles away from the light source towards the focus spot [3]. Local confinement of gradient force is determined by wavelength and numerical aperture of objective lens, in this case, about 1 μm, so that the contribution of gradient force to particle migration is spatially limited. This is theoretically well recognized but directly confirmed here for the first time by wide-filed Rayleigh scattering imaging, on which we propose that scattering force has an important role for understanding nanomaterial trapping when appreciable convection flow due to local heating is suppressed. On the other hand, when we shifted the observation plane to +20 μm from the focus spot, particle-deficient area was not clearly observed (Fig. 2(e)). It can be assumed that the continuously transferred particles from the lower position are supplied to the area. Moreover, this position which is far from to the bottom surface of the substrate compared to other positions of −20 to −60 μm, so that diffusion of nanoparticles might be different from each other. At the present stage of investigation, we cannot explain well the result of Fig. 2(e), and more detailed experimental and theoretical works including systematic analysis of distribution at diffusion in the wide-field images are being started in our laboratory.

The observed laser trapping of gold nanoparticles indicates that the gradient force overcomes the scattering force at the laser focus spot. Here let us estimate the both forces acting on gold nanoparticles. Theoretically, when photon pressure is exerted on nanomaterials, i.e., Rayleigh particles that are smaller than the wavelength of laser light, the total force acting on the trapped particles can be written as follows [28].

$$F = \frac{1}{2}\varepsilon_m \alpha \nabla E^2 + \frac{n_m \left\langle E \times B \right\rangle C_{sca}}{c} \quad (1)$$

where E and B denote the electric field and magnetic flux density, respectively, and ∇ represents a gradient with respect to the spatial coordinates. ε_m, n_m, C_{scat} and c represent the permittivity of the surrounding medium, its refractive index, light scattering cross section of the particle, and speed of light in vacuum, respectively. The polarizability of the particle, α, under the dipole approximation is given by

$$\alpha = 4\pi r^3 \frac{(n_p/n_m)^2 - 1}{(n_p/n_m)^2 + 2} \quad (2)$$

where r, and n_p are the radius of the particle and the refractive index of the particle, respectively. The gradient force of photon pressure is described as the first term of Eq. (1). The scattering force to the particle, which is given in the second term of Eq. (1), is derived from the change in the direction of the Pointing vector of the electromagnetic wave. As expressed in Eq. (1), the gradient force is proportional to the gradient of light intensity and points in the direction of the intensity gradient, while the scattering force is proportional to the Pointing vector and the direction is along the beam direction.

As shown in Eq. (1), the gradient force F_{grad} is proportional to the power of the electric field gradient ∇E^2. In polar coordinate system, the electric filed $E(r,z)$ is connected to the light intensity distribution $I(r,z)$ as follows [28].

$$I = \frac{n_m \varepsilon_0 c}{2} \left| E \right|^2 \quad (3)$$

The light intensity distribution of a focused light around the focus $I(r,z)$ is expressed in the Gaussian–Lorentzian form as follows.

$$I(r,z) = \frac{2P}{\pi \omega_r^2} \exp\left(-\frac{2r^2}{\omega_r^2}\right) \quad (4)$$

where P and ω_r denote laser power and beam radius at the waist in lateral, respectively. At trapping wavelength $\lambda = 1064$ nm and numerical aperture of objective lens $NA = 0.9$, we determined ω_r as 600 nm. The complex refractive index of gold at 1064 nm is set to 0.0466 + 7.6144i from a literature by Johnson and Christy [29]. The scattering cross section of a gold nanoparticle with 60 nm-diameter embedded in a medium whose refractive index is 1.33 is calculated as 0.313×10^{-16} m^2 on the basis of Mie theory [30]. We also use the effective volume of gold nanoparticle by taking into account its skin depth 23 nm [31].

Employing these parameters listed above, we calculated the maximum gradient and scattering force at 700 mW irradiation based on Eq. (1). The maximum value of the gradient force was estimated to be 3.1 pN for the lateral direction. The gradient force possesses a vertical component too, but it should be much smaller than the lateral one because of the less gradient in the vertical dimension. Meanwhile, the scattering force at the focus spot was calculated to be 0.17 pN. It is important to note that the scattering force shows mainly a vertical component because the direction is parallel to the Pointing vector. As the calculation indicates that the gradient force near the focus spot is much larger than the scattering force, it supports the experimental result that gold nanoparticles could be trapped stably at the focus spot. It is also noteworthy that Eq. (1) denotes that the scattering force show easy slope in the irradiated domain compared to the gradient force. Because the scattering force is linear to the light intensity and the vertical incline in the light intensity is gentle as indicated in Eq. (4), the acting area of scattering force should be wider in lateral and much deeper in vertical direction compared to that of the gradient force. Furthermore,

Eq. (1) also implies that the gradient force is linear to the polarizability of particle and the scattering force is linear to the scattering cross section of the particle. In Rayleigh particle, the scattering cross section is proportional to the square of polarizability. So, in metallic nanoparticle which tend to exhibit higher poralizability compared to dielectric particle, a contribution of the scattering force can be enhanced when their diameters are identical in both metallic and dielectric particles each other.

Next, we describe light scattering spectra of gold nanoparticles and their temporal intensity change at the focus position. Initially, we sequentially measured light scattering spectra series by setting acquisition time to 500 ms for each spectrum. The measurement was started after we observed steady-state laser trapping at the focus spot as shown in Fig. 2(a). The light scattering spectral intensity at 550 nm were recorded up to 100 s from nanoparticle trapping and the intensity at 550 nm is plotted against time in Fig. 3(a). It is obvious that the intensity drastically fluctuates depending on time, which is consistent with the fluctuation of the intensity at the focal point in the wide-field image (Fig. 2(a)). The nanoparticle concentration of the present solution guarantees that the nanoparticles are dispersed individually and the light scattering intensity without trapping laser irradiation is below 100, as shown in Fig. 3(a). This represents average intensity due to migration of individual nanoparticles, and its histogram is included in Fig. 3(b). Thus, it can be assumed that the intensity is proportional to the number of trapped particles and intensity fluctuation represents trapping and detrapping at the focus point. The histogram of Fig. 3(b) shows three peaks around 200, 350, and 500, which are indicated as A, B, and C, respectively. The occurrence of A, B, and C decreases in this order, and the frequency around peak C scatters compared to that of peaks A and B. Therefore, these peaks are supposed to reflect the respective number of trapped particles. The lowest intensity peak A with the highest frequency of occurrence means single particle trapping, and the second B means simultaneous trapping of two particles, and eventually the highest intensity peak corresponds to three particles trapping.

The peak intensity values of 200, 350, and 500, however, are not linear to the number of trapped particles of 1, 2, and 3, which is considered from two reasons. The first is concerned with measurement condition. The time width during which 2 or 3 nanoparticle are simultaneously trapped at the focus point is shorter than that of single particle trapping. Once several numbers of particles are trapped in small volume, they receive repulsive force and are prevented from stable trapping, resulting in the further short lifetime of the assembly. Furthermore, their staying time at the focus should be short compared to the data acquisition time, 500 ms. The second is due to light scattering spectral modification due to electromagnetic interaction among gold nanoparticles. Fig. 3(c) represents typical three light scattering spectra of each intensity step (A, B, and C) shown in Fig. 3(b) at the trapping laser focus spot. All the spectra exhibit strong light scattering band around 550 nm, which is assigned to localized plasmon resonance of gold nanoparticles. With increasing the intensity, peak wavelength shifts from 550 to 565 nm and an additional band appears around 720 nm, while the ratio between the primary and additional bands is increased from about 0.2 to 0.7. This is explained in terms of particle–particle electromagnetic interaction [31] exerted by optical binding in the laser trapping [32] since similar result was reported previously [8]. This can be considered to be interaction among nanoparticles at the focus, and the appearance of the additional band, thus, the interaction can induce the intensity decrease of the primary plasmon band, 550 nm. This is another reason why a linear relation does not hold among peak intensities of A, B, and C in Fig. 3(b). These considerations support the large width of peak C in the histogram (Fig. 3(b)) compared to those of A and B. Consequently, we can conclude that laser trapping of gold nanoparticles at the focus spot induces their assembling and the number of trapped particles is three at most on 700 mW irradiation. Recently, Ohlinger et al. demonstrated laser trapping of silver nanoparticles by 808 nm CW laser and found that multiple particles up to four are trapped [33]. They also revealed that the optically trapped-multiple silver nanoparticles show such nonlinear spectral shape change depending on the number of trapped particle, similarly to our results. Changes in the number of trapped particle and the geometrical structure of the formed assembly modify the resonance mode and its intensity. Especially in three particles trapping, the three-body interaction in the confined space would be complex.

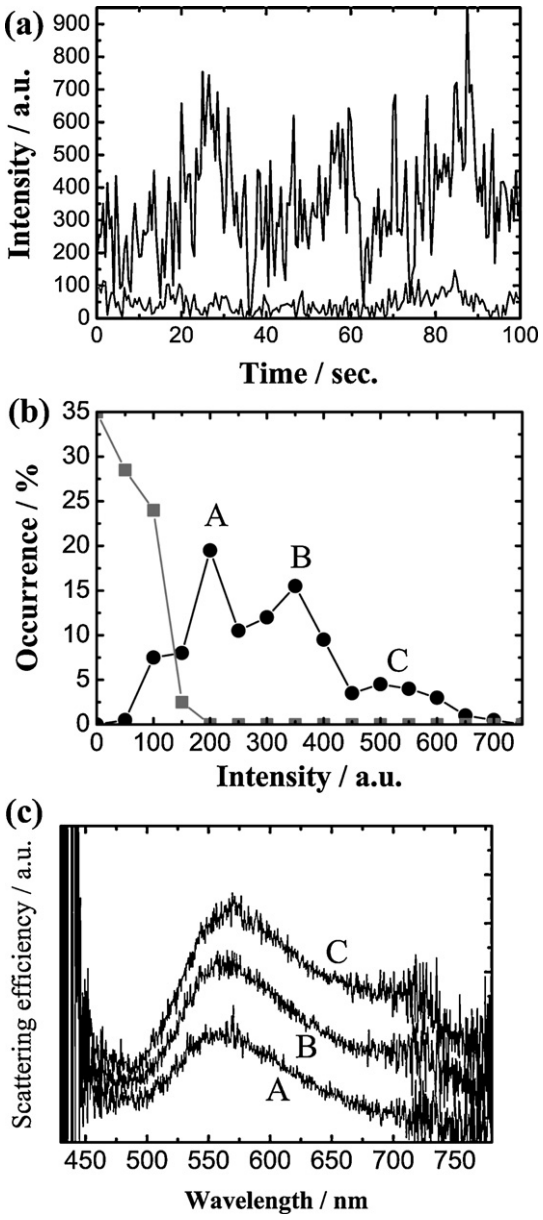

Fig. 3. Light scattering spectra and their temporal change of gold nanoparticles in heavy water at the trapping laser focus spot. The focus height from the substrate and the trapping laser power were 100 μm and 700 mW, respectively. (a) Temporal change of light scattering spectral intensity at 550 nm with (black line) and without (gray line) trapping laser irradiation, where acquisition time is 500 ms. (b) Intensity histograms summarized from (a), where the occurrence was counted for every 50 intensity (a.u.) interval of (a). Black line with closed circular makers was obtained with trapping laser irradiation, while gray line with closed square makers was without irradiation. (c) Three examples of light scattering spectra at the trapping laser focus spot taken as a function of light scattering intensity, where A, B, and C in (c) correspond to A, B, C in (b), respectively.

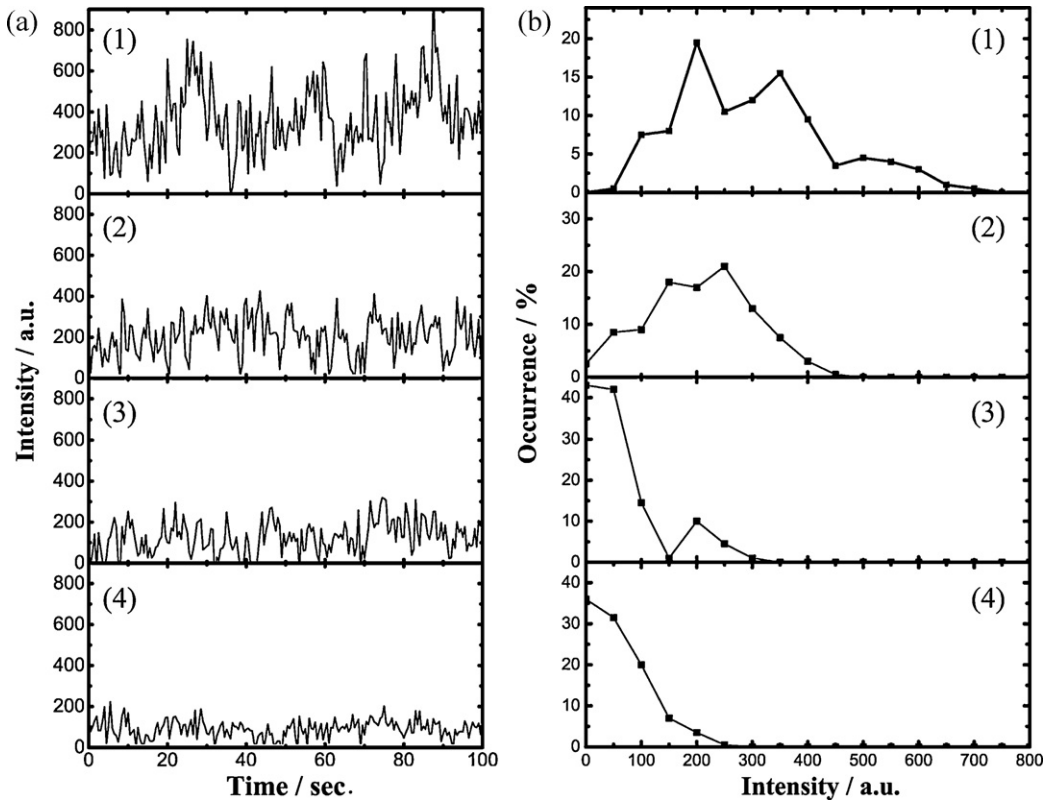

Fig. 4. Lateral distance dependence of temporal change in light scattering spectral intensity of gold nanoparticles in D_2O under laser trapping with 700 mW. The laser focus height from the substrate was fixed at 100 μm above. The lateral distances from the focus point were set to (1) 0 μm, (2) 0.7 μm, (3) 1.4 μm, and (4) 2.8 μm, respectively. The data acquisition procedure is common to the experiment shown in Fig. 3. (a) Temporal changes of light scattering spectral intensity at 550 nm. (b) Intensity histogram summarized from (a). Same figures to Fig. 3(b) and (c) are displayed here as (1) for comparison.

Similarly, we followed temporal change in light scattering spectrum at different positions with shifting the observation point from the laser focus to the surrounding area by utilizing galvano mirrors. This enables us to evaluate distance dependence of the particle existence probability upon laser trapping. Fig. 4(a) shows temporal change of the scattering intensity of 550 nm at different distance from the focus, and its histogram at each position is summarized in Fig. 4(b). To avoid overlap of observation areas, namely double counting, the distance between the points was set to 700 nm which is larger than the spatial resolution of our instrument (500 nm for lateral). Moreover, it should be noted that the area of the histogram shown in Fig. 3(b) can reflect average number of existing particles at the observation points, i.e., particle existence probability. It is obvious that light intensity and its fluctuation become weaker and smaller, respectively, with increasing the distance from the focus spot, which means that the number of particles is decreased with distance. As the result, we successfully evaluated the particle existence probability, namely, particle distribution depending on the lateral distance from the focus spot can be directly made clear by wide-field Rayleigh scattering spectroscopy.

The spatial distribution of gold nanoparticles in D_2O during laser trapping, namely, the lateral distance dependence of particle existence probability around the trapping laser focus at 700 mW is shown in Fig. 5(a). The particle existence probability is calculated based on the area of light scattering intensity histogram shown in Fig. 4(b). The probability is highest at the focus, which is of course explained in view of laser trapping due to gradient force. The number of the particles at the focus spot is sometimes three as discussed before, while it decreases rapidly with the distance. The profile shows a Gaussian-shape distribution and the probability is almost zero at about 2 μm far from the focus. Without laser irradiation, the scattering light intensity is almost zero because particles seldom cross the focus point.

In order to evaluate the distance dependence of particle existence probability around the trapping laser focus, photon pressure potential is calculated considering the optical condition of this experimental setup. When the scattering force acting on the particle is much smaller than the gradient force, the photon pressure potential U in lateral focus plane is governed by the gradient force and is expressed as a function of the distance r from the focus spot,

$$U = -\frac{1}{2}\varepsilon_m \alpha \left|E\right|^2 \tag{5}$$

The calculated photon pressure based on Eqs. (3)–(5) is shown in Fig. 5(b).

Firstly, the calculated depth of the potential at the focus spot is much larger than the thermal energy k_bT, where k_b and T are the Boltzmann constant and absolute temperature of the particle, respectively. This also supports that the laser trapping at the focus spot is stable against thermal motion of the particle. Secondly, the Gaussian profile of the photon pressure potential well reproduces qualitatively the spatial profile of particle existence probability in D_2O. However, the full width of the calculated potential profile is not large than 2 μm, and is less than experimentally obtained one, ~4 μm. Even considering the spatial resolution of the experimental setup, the experimental width seems to be larger than the predicted width. On the other hand, the displacement measurement using a quadrant photodetector by Hansen et al. revealed that Brownian motion of the trapped single-nanoparticle well reproduces the theoretically predicted potential [34]. Since we trapped gold nanoparticles up to three, the broadening of the potential curve compared to the single particle trapping could be considered in

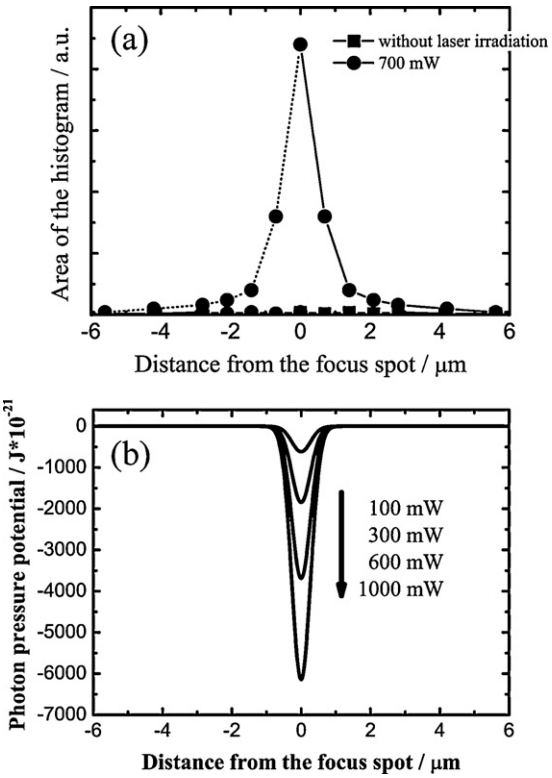

Fig. 5. (a) Spatial distribution of gold nanoparticle distribution in D_2O with and without trapping laser at 700 mW. The vertical axis represents the area of the corresponding intensity histogram of Fig. 4(b). The minus region of the lateral axis is a mirror image of the positive region. (b) Calculated spatial profile of photon pressure potential at the focus plane with 100, 300, 600, and 1000 mW of laser power focused by an objective lens with NA 0.9.

terms of the optical binding [32]. However, the single particle trapping is the most stable and the lifetime of the multiple particle trapping is shorter compared to the data acquisition time, so that theoretical estimation considering the optical binding effect may not give so large broadening of the experimental curve. Alternatively, escaping of nanoparticles due to relatively shallow potential or/and the scattering force may result in the broadening of the potential. This is consistent with the in situ observation of the laser trapping process with wide-field imaging technique shown in Fig. 2. This consideration on the lateral particle distribution is being examined by changing sample concentration, trapping laser power, and optical parameters, on which more reliable picture will be reported in near future.

4. Conclusion

We have investigated laser trapping and assembling process of gold nanoparticles in D_2O by using wide-field Rayleigh scattering illumination. It helps us to visualize particle motion at single nanoparticle level not only at the laser focus spot but also in the surroundings. It is clearly shown that scattering force induced by the focused laser beam can assist particle migration inside the optical cone of the laser light to the laser focus spot. We also evaluated the lateral distribution of the particle existence probability from the focus spot and clarified the role of the photon pressure in terms of gradient and scattering forces. The present results are obtained only for heavy water solution where local heating by 1064 nm irradiation is suppressed efficiently. Thus characteristics of laser trapping assembling of gold nanoparticles by photon pressure have been made clear here for the first time.

Recently, our group reported that glycine clusters in D_2O solution form the millimeter-sized domain upon tightly focused laser irradiation [35]. We understand that the laser-induced phenomenon is not explained only in terms of photon pressure. Glycine clusters should be supplied to the focus spot from its surrounding by diffusion, which is now considered to be caused by surface morphology change and accompanying convection. This behavior will be also observed and analyzed by the wide-field Rayleigh scattering imaging. The present study is a milestone in the systematic studies to understand dynamics of such nano- or molecular assembling and crystallization by tightly focused laser.

Acknowledgements

We thank Dr. Anwar Usman for the proofreading. The present work was partially supported by the MOE-ATU Project (National Chiao Tung University) from the Ministry of Education of Taiwan, the National Science Council of Taiwan to T.U. (NSC 98-2113-M-009-013-MY2) and to H.M. (NSC 98-211-M-009-001), and a KAKENHI grant (a Grant-in-Aid for Scientific Research) in the Priority Area “Molecular Science for Supra Functional Systems” (19056009) to T.U., “Strong Photon-Molecule Coupling Fields” (21020022) to T.S. from the Ministry of Education, Culture, Sports, Science and Technology of Japan (MEXT), a KAKENHI (C) grant (20550136) to T.S., and a KAKENHI (S) grant (18106002) to H. M. from the Japan Society for the Promotion of Science (JSPS).

References

[1] A. Ashkin, Phys. Rev. Lett. 24 (1970) 156.
[2] A. Ashkin, J.M. Dziedzic, J.E. Bjorkholm, S. Chu, Opt. Lett. 11 (1986) 288.
[3] A. Ashkin, Biophys. J. 61 (1992) 569.
[4] A. Ashkin, Proc. Natl. Acad. Sci. U.S.A. 94 (1997) 4853.
[5] H. Masuhara, F.C.D. Schryver (Eds.), Mesoscopic Chemistry: A Chemistry for the 21st Century., Black-well Science, Oxford, 1999.
[6] H. Masuhara, H. Nakanishi, K. Sasaki (Eds.), Single Organic Nanoparticles., Springer-Verlag, NY, 2003.
[7] D.G. Grier, Nature 424 (2003) 810.
[8] H. Yoshikawa, T. Matsui, H. Masuhara, Phys. Rev. E 70 (2004) 061406.
[9] J. Prikulis, F. Svedberg, M. Kall, J. Enger, K. Ramser, M. Goksor, D. Hanstorp, Nano Lett. 4 (2004) 115.
[10] F. Svedberg, Z. Li, H. Xu, M. Kall, Nano Lett. 6 (2006) 2639.
[11] C. Hosokawa, H. Yoshikawa, H. Masuhara, Phys. Rev. E 72 (2005) 021408.
[12] P.J. Pauzauskie, A. Radenovic, E. Trepagnier, H. Shroff, P. Yang, J. Liphardt, Nat. Mater. 5 (2006) 97.
[13] P. Borowicz, J. Hotta, K. Sasaki, H. Masuhara, J. Phys. Chem. B 102 (1998) 1896.
[14] T.A. Smith, J. Hotta, K. Sasaki, H. Masuhara, Y. Itoh, J. Phys. Chem. B 103 (1999) 1660.
[15] S. Masuo, H. Yoshikawa, H.-G. Nothofer, A.C. Grimsdale, U. Scherf, K. Mullen, H. Masuhara, J. Phys. Chem. B 109 (2005) 6917.
[16] Y. Nabetani, H. Yoshikawa, A.C. Grimsdale, K. Müllen, H. Masuhara, Jpn. J. Appl. Phys. 46 (2007) 449.
[17] W. Singer, T.A. Nieminen, N.R. Heckenberg, H. Rubinsztein-Dunlop, Phys. Rev. E 75 (2007) 011916.
[18] Y. Tsuboi, T. Shoji, N. Kitamura, Jpn. J. Appl. Phys. 46 (2007) L1234.
[19] Y. Tanaka, H. Yoshikawa, H. Masuhara, J. Phys. Chem. B 110 (2006) 17906.
[20] Y. Tsuboi, T. Shoji, N. Kitamura, J. Phys. Chem. C 114 (2009) 5589.
[21] T. Sugiyama, T. Adachi, H. Masuhara, Chem. Lett. 36 (2007) 1480.
[22] T. Rungsimanon, K. Yuyama, T. Sugiyama, H. Masuhara, Cryst. Growth Des. 10 (2010) 4686.
[23] Y. Jiang, T. Narushima, H. Okamoto, Nat. Phys. 6 (2010) 1005.
[24] Y. Tanaka, H. Yoshikawa, T. Itoh, M. Ishikawa, J. Phys. Chem. C 113 (2009) 11856.
[25] E. Messina, E. Cavallaro, A. Cacciola, M.A. Iati, P.G. Gucciardi, F. Borghese, P. Denti, R. Saija, G. Compagnini, M. Meneghetti, V. Amendola, O.M. Marago, ACS Nano 5 (2011) 905.
[26] T. Uwada, T. Sugiyama, A. Miura, H. Masuhara, Proc. SPIE 7762 (2010) 77620N.
[27] T. Uwada, R. Toyota, H. Masuhara, T. Asahi, J. Phys. Chem. C 111 (2007) 1549.
[28] Y.R. Shen, The Principles of Nonlinear Optics, Wiley, NY, 1984, 366.
[29] P.B. Johnson, R.W. Christy, Phys. Rev. B 6 (1972) 4370.
[30] C.F. Bohren, D.R. Huffman, Absorption and Scattering of Light by Small Particles, Wiley, NY, 1983.
[31] U. Kreibig, M. Vollmer, Optical Properties of Metal Clusters, Springer, Berlin, 1995.
[32] P.C. Chaumet, M. Nieto-Vesperinas, Phys. Rev. B 64 (2001) 035422.
[33] A. Ohlinger, S. Nedev, A.A. Lutich, J. Feldmann, Nano Lett. 11 (2011) 1770.
[34] P.M. Hansen, V.K. Bhatia, N. Harrit, L. Oddershede, Nano Lett. 5 (2005) 1937.
[35] K. Yuyama, T. Sugiyama, H. Masuhara, J. Phys. Chem. Lett. 1 (2010) 1321.